Supplementary information for
"Multiscale Design of Two-Dimensional MoS_3 Materials and Their Electrocatalytic Performance for CO_2 Reduction"

HuiLi Li[a,b], JinRong Huo[a], Chenxu Zhao[a], JinRong Li[a], Chaozheng He[a*]

[a] *Institute of Environmental and Energy Catalysis, School of Materials Science and Chemical Engineering, Xi'an Technological University, Xi'an 710021, PR China*
[b] *Shanxi University of Electronic Science and Technology, Linfen, 041000, PR China*

The optical properties of monolayer MoS_3, including the absorption coefficient α(ω), real and imaginary parts of the dielectric function $\varepsilon_1(\omega)$ and $\varepsilon_2(\omega)$, reflectivity, and transmittance, using the following equations:

$$\varepsilon_1(\omega) = 1 + \frac{2}{\pi} P \int_0^{\infty} \frac{\varepsilon_2^{\alpha\beta}(\omega')\omega'}{\omega'^2 - \omega^2} d\omega' \qquad \text{Equation S1}$$

$$\varepsilon_2(\omega) = \frac{4\pi^2 e^2 \hbar^2}{\Omega \omega^2 m_e^2} \lim_{q \to 0} \sum_{c,v,k} 2\omega_k \delta\left(\epsilon_{ck+q} - \epsilon_{vk} - \omega\right) \qquad \text{Equation S2}$$

$$\alpha(\omega) = \sqrt{2}\omega \left\{ \left[\varepsilon_1^2(\omega) + \varepsilon_2^2(\omega)\right]^{\frac{1}{2}} - \varepsilon_1(\omega) \right\}^{\frac{1}{2}} \qquad \text{Equation S3}$$

$$R(\omega) = \left[\frac{\sqrt{\varepsilon_1(\omega) + i\varepsilon_2(\omega)} - 1}{\sqrt{\varepsilon_1(\omega) + i\varepsilon_2(\omega)} + 1} \right]^2 \qquad \text{Equation S4}$$

$$T(\omega) = \frac{(1 - R(\omega))^2 e^{-\alpha(\omega)d}}{1 - R(\omega)^2 e^{-2\alpha(\omega)d}} \qquad \text{Equation S5}$$

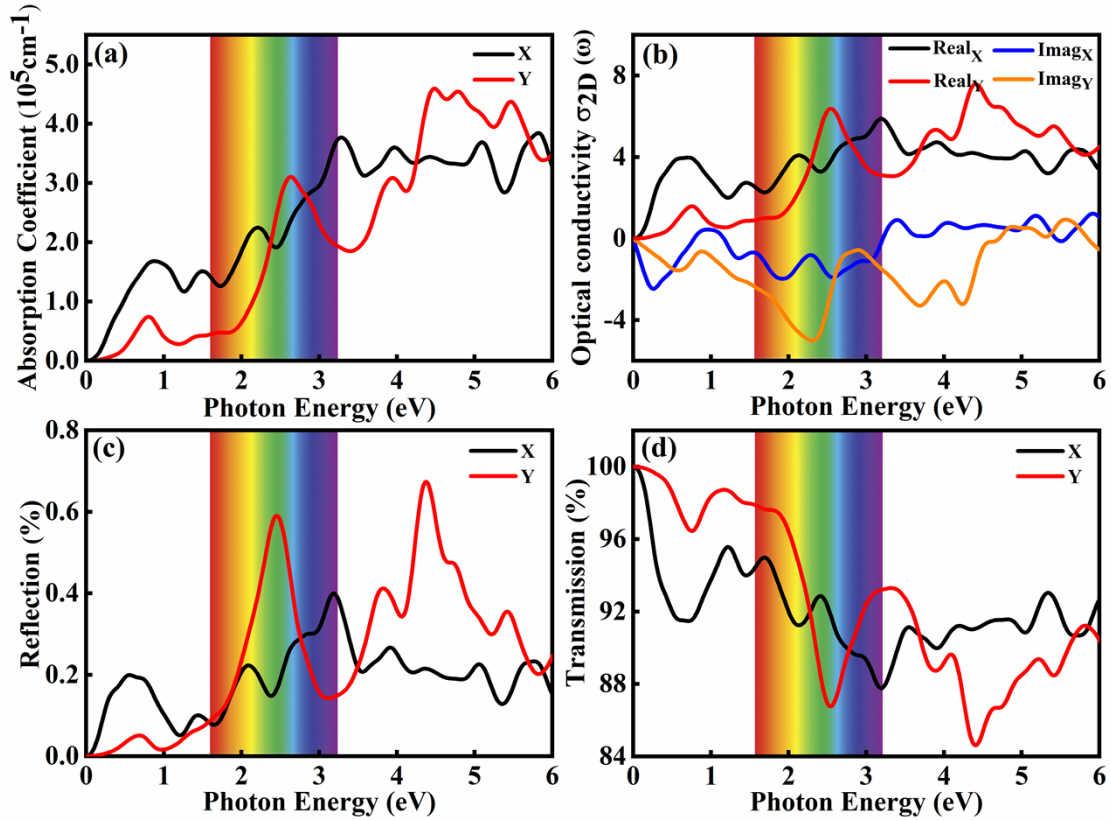

Fig. S1 (a) Absorption coefficient of monolayer MoS_3; (b) Real and imaginary parts of the dielectric function; (c) Reflectivity; (d) Transmittance.

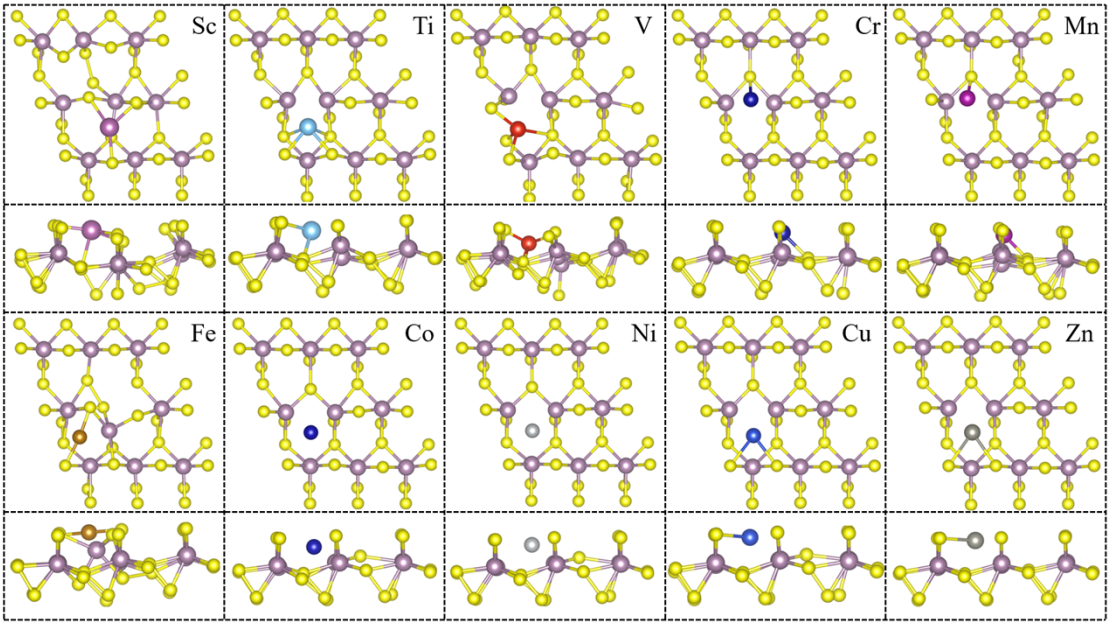

Fig. S2 Top and side views of the most stable structures of MoS_3 doped with transition metal atoms (Sc–Zn) at the α site.

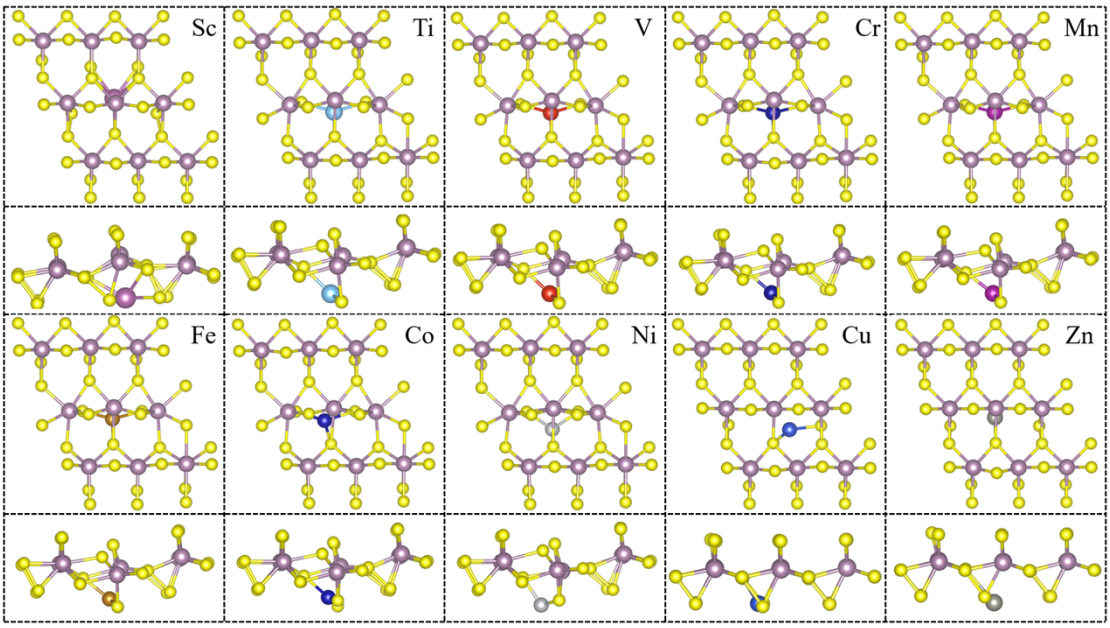

Fig. S3 Top and side views of the most stable structures of MoS_3 doped with transition metal atoms (Sc–Zn) at the β site.

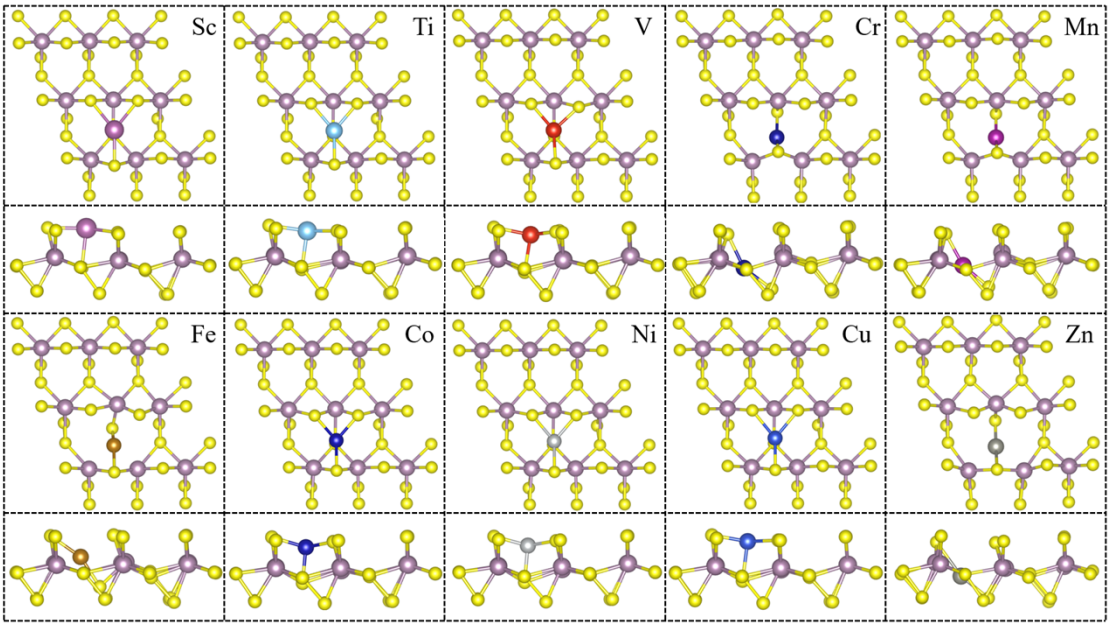

Fig. S4 Top and side views of the most stable structures of MoS_3 doped with transition metal atoms (Sc–Zn) at the γ site.

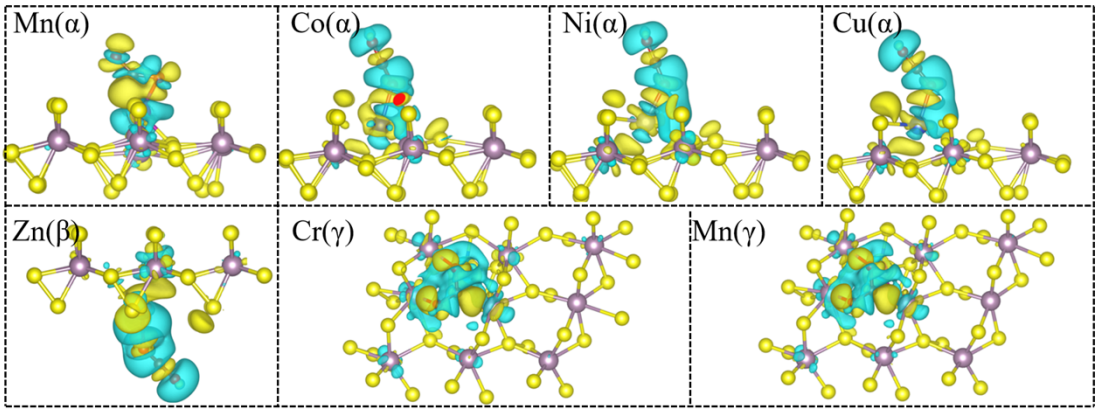

Fig. S5 Charge density difference (CDD) plots of the most stable CO_2 adsorption configurations on M_α@MoS_3, M_β@MoS_3, and M_γ@MoS_3 (M_α: Mn, Co, Ni, Cu; M_β: Zn; M_γ: Cr, Mn). Yellow and cyan regions indicate charge accumulation and depletion, respectively. The isosurface value is set to 0.08.

Table S1 Calculated structural parameters (lattice constants and atomic coordinates) for the predicted stable and metastable phases of MoS_3

Phase	**Lattice parameters(Å, °)**	**Atomic coordinates (x, y, z)**
Stable Phase	a = 3.23 Å b = 4.35 Å α = 90.35° β = 91.96° γ = 111.68°	Mo : 0.58 0.82 0.51 S1 : 0.28 0.24 0.49 S2 : 0.41 0.53 0.42 S3 : 0.10 0.82 0.58
Metastable Phase	a = 4.55 Å b = 4.30 Å α = 90.56° β = 90.78° γ = 90.01°	Mo : 0.37 0.94 0.48 S1 : 0.51 0.43 0.45 S2 : 0.92 0.93 0.45 S3 : 0.35 0.94 0.58
	a = 8.25 Å b = 3.16 Å α = 90.00° β = 94.44° γ = 90.00°	Mo1 : 0.14 1.00 0.55 Mo2 : 0.64 0.50 0.55 S1 : 0.02 0.50 0.47 S2 : 0.78 0.50 0.45 S3 : 0.85 0.00 0.59 S4 : 0.52 0.00 0.47 S5 : 0.27 0.00 0.45 S6 : 0.34 0.50 0.59

Table S2 Bond Angle (A_B,) of CO_2 Adsorbedon $M@MoS_3$ with the Most Stable Confguration

M@MoS$_3$	**A_B (∠OCO, °)**	**M@Cu(211)**	**A_B (∠OCO, °)**	**M$_2$@C$_2$N**	**A_B (∠OCO, °)**
$Mn_\alpha@MoS_3$	142.8°	Y@Cu(211)	127.7°	FeFe@C_2N	130.5°
$Co_\alpha@MoS_3$	1797°	Fe@Cu(211)	140.1°	FeCo@C_2N	131.0°
$Ni_\alpha@MoS_3$	179.5°	Co@Cu(211)	140.1°	FeNi@C_2N	132.7°
$Cu_\alpha@MoS_3$	179.7°	Ni@Cu(211)	142.4°	FeCu@C_2N	132.8°
$Zn_\beta@MoS_3$	179.3°	Ru@Cu(211)	139.0°	CuCo@C_2N	135.0°
$Cr_\gamma@MoS_3$	116.6°	Rh@Cu(211)	140.2°	CuNi@C_2N	133.6°
$Mn_\gamma@MoS_3$	116.5°	Pt@Cu(211)	137.8°	CuCu@C_2N	136.6°

Table S3 Calculated total energy (E), zero-point energy (E_{ZPE}), entropy (S), and Gibbs free energy (G) for various adsorbed species on $Mn_\alpha@MoS_3$.

Species	***E* (eV)**	***E*$_{ZPE}$ (eV)**	***TS* (eV)**	***G* (eV)**
*CO_2	-251.9789174	0.307395	0.208416	-251.8799384
*COOH	-255.9454814	0.611309	0.219569	-255.5537414
*HCOO	-256.1216625	0.581241	0.176474	-255.7168955
*HCOOH	-260.1017699	0.916383	0.183188	-259.3685749
*CHO	-248.0707252	0.497841	0.159476	-247.7323602
*CHOH	-252.3032121	0.777727	0.170056	-251.6955411
*CH_2O	-252.4498495	0.800999	0.115108	-251.7639585
*CH	-240.328257	0.371913	0.061938	-240.018282
*CH_2OH	-256.248121	1.106467	0.166535	-255.308189
*CH_2	-244.3191822	0.623603	0.098457	-243.7940362
*CH_3OH	-260.4658063	1.410755	0.22249	-259.2775413
*CH_3	-248.1324117	0.89704	0.162132	-247.3975037
*OH	-239.8417103	0.327524	0.125372	-239.6395583
*CH_4	-253.1584424	1.203737	0.162024	-252.1167294
*H_2O	-243.6074319	0.839214	0.0898	-242.8580179

Table S4 Calculated total energy (E), zero-point energy (E_{ZPE}), entropy (S), and Gibbs free energy (G) for various adsorbed species on $Co_\alpha@MoS_3$.

Species	***E* (eV)**	***E*$_{ZPE}$ (eV)**	***TS* (eV)**	***G*$_{corr}$ (eV)**
*CO_2	-250.6508129	0.327568	0.195635	-250.5188799
*COOH	-253.9611377	0.606295	0.238351	-253.5931937
*HCOO	-254.0947654	0.588369	0.215875	-253.7222714
*HCOOH	-258.4748747	0.923794	0.227663	-257.7787437

Table S5 Calculated total energy (E), zero-point energy (E_{ZPE}), entropy (S), and Gibbs free energy (G) for various adsorbed species on Ni_{α}@MoS_3

Species	***E* (eV)**	E_{ZPE} **(eV)**	***TS* (eV)**	G_{corr} **(eV)**
*CO_2	-249.6879779	0.323813	0.200853	-249.5650179
*COOH	-253.2966594	0.607386	0.236596	-252.9258694
*HCOO	-253.6453797	0.615536	0.212275	-253.2421187
*HCOOH	-257.2860207	0.92945	0.287361	-256.6439317

Table S6 Calculated total energy (E), zero-point energy (E_{ZPE}), entropy (S), and Gibbs free energy (G) for various adsorbed species on Zn_{β}@MoS_3

Species	***E* (eV)**	E_{ZPE} **(eV)**	***TS* (eV)**	G_{corr} **(eV)**
*CO_2	-246.9279086	0.318795	0.224447	-246.8335606
*COOH	-250.2347355	0.596367	0.134835	-249.7732035
*HCOO	-250.5798334	0.589205	0.162186	-250.1528144
*CO	-239.037729	0.17575	0.135238	-238.997217
*HCOOH	-254.7820726	0.926203	0.167932	-254.0238016
*CHO	-242.2623094	0.452231	0.147534	-241.9576124
*CHOH	-245.7633416	0.796852	0.157375	-245.1238646
*CH_2O	-246.6926212	0.774729	0.181969	-246.0998612
*CH_2OH	-250.2076108	1.085824	0.172844	-249.2946308
*CH_3O	-250.566701	1.075891	0.259719	-249.750529
*CH_2	-239.3476968	0.659868	0.054825	-238.7426538
*CH_3OH	-255.044067	1.410699	0.217151	-253.850519
*O	-230.0821442	0.077459	0.042296	-230.0469812
*CH_3	-243.2397683	0.93013	0.127158	-242.4367963
*OH	-233.7755562	0.441062	0.090515	-233.4250092
*CH_4	-247.205095	1.212648	0.252688	-246.245135
*H_2O	-238.1951738	0.741111	0.144134	-237.5981968

.

Table S7 Reaction free energies (ΔG_r) for different steps in TM@MoS_3 systems.

ΔG_r (eV)	**Mn_{α}@Mo_{S3}**	**Co_{α}@Mo_{S3}**	**Ni_{α}@Mo_{S3}**	**Zn_{β}@Mo_{S3}**
*CO_2 → *COOH	-0.21	0.39	0.10	0.52
*CO_2 → *HCOO	-0.38	0.26	-0.22	0.14（0.80）
*COOH → *CO	-0.94	—	—	-0.42
*HCOO → *HCOOH	-0.19	-0.60	0.06	-0.41

*COOH → *HCOOH	-0.35	—	—	-0.79
*CO → *CHO	—	—	—	0.50
*HCOOH → *CHO	0.44	—	—	
*CHO→*CHOH	-0.50	—	—	0.29
CHO→CH_2O	-0.57	—	—	-0.68
*CHOH → *CH	0.49	—	—	
*CHOH → *CH_2OH	-0.15	—	—	-0.71
*CH_2O → *CH_2OH	-0.08	—	—	0.27
*CH_2O → *CH_3O	—	—	—	-0.19
*CH → *CH_2	-0.32	—	—	
*CH_2OH → *CH_2	0.32	—	—	-0.63
*CH_2OH → *CH_3OH	-0.51	—	—	-1.09
*CH_3O → *CH_3OH	—	—	—	-0.63
*CH_3O → *O	—	—	—	-0.33
*CH_2 → *CH_3	-0.14	—	—	-0.23
*CH_3OH → *CH_3	-0.11	—	—	0.29
*CH_3OH →*OH	-0.39	—	—	0.40
*O →*OH	—	—	—	0.10
*CH_3 → *CH_4	-0.46	—	—	-0.35
*OH → *H_2O	0.25	—	—	-0.72

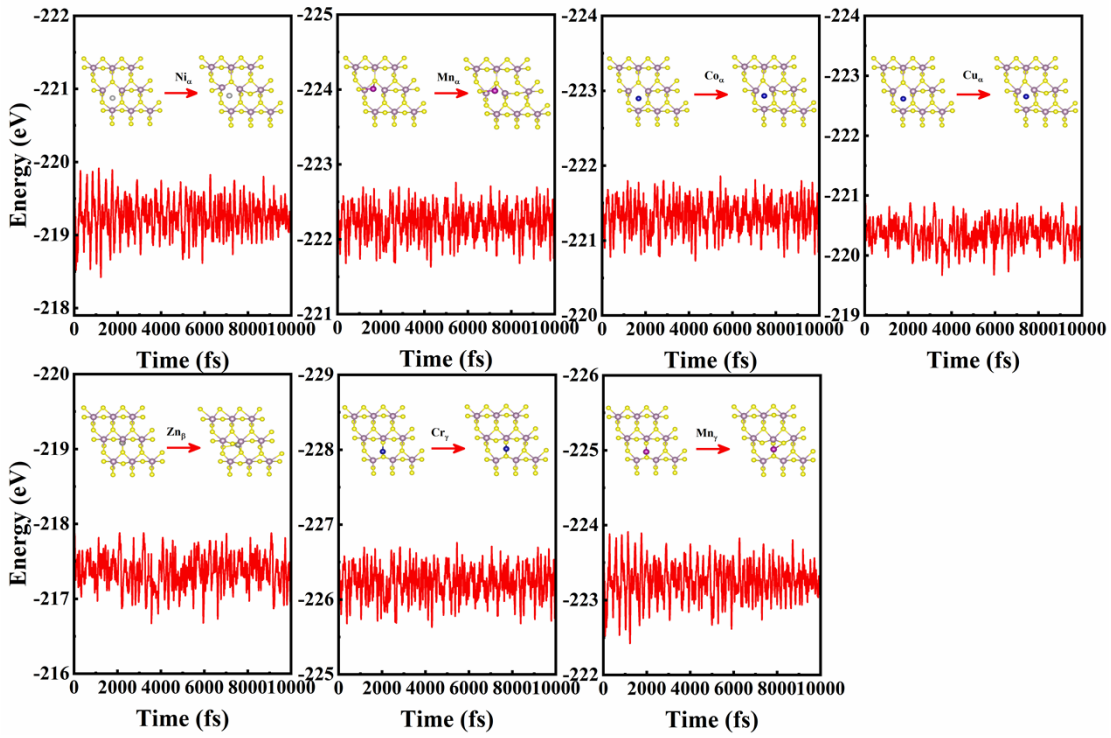

Fig. S6 Molecular dynamics simulation diagram of $MnS_\alpha@MoS_3$, $CoS_\alpha@MoS_3$, $NiS_\alpha@MoS_3$, $CuS_\alpha@MoS_3$, $ZnS_\beta@MoS_3$, $CrS_\gamma@MoS_3$ and $MnS_\gamma@MoS_3$ at 300 K.

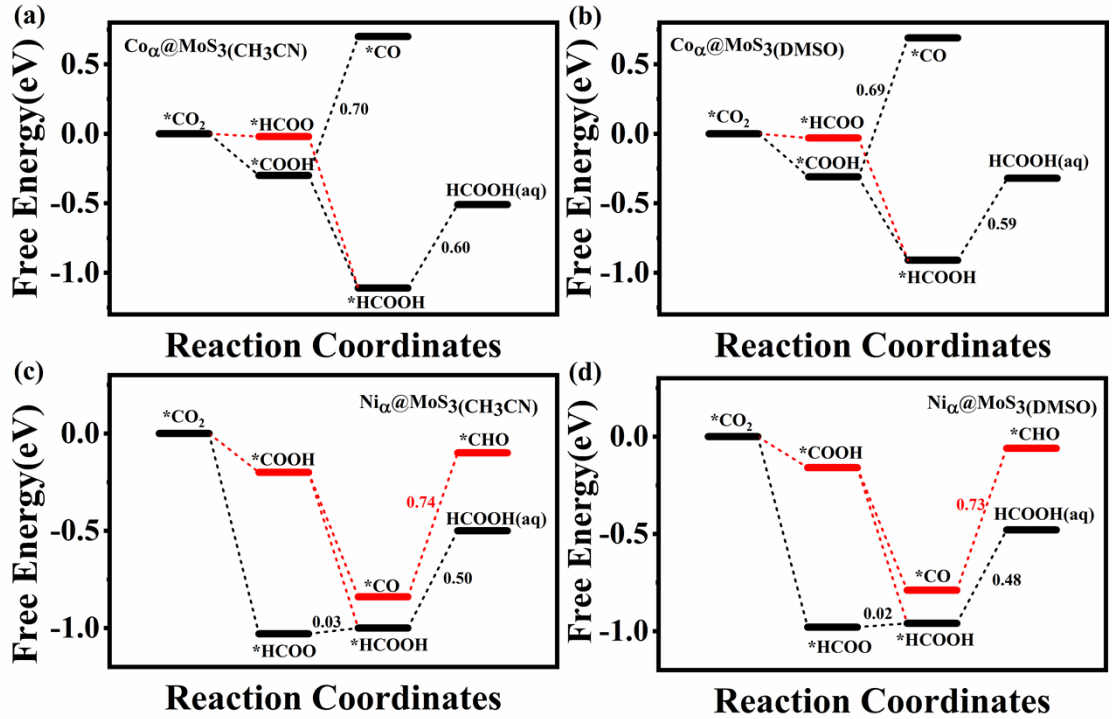

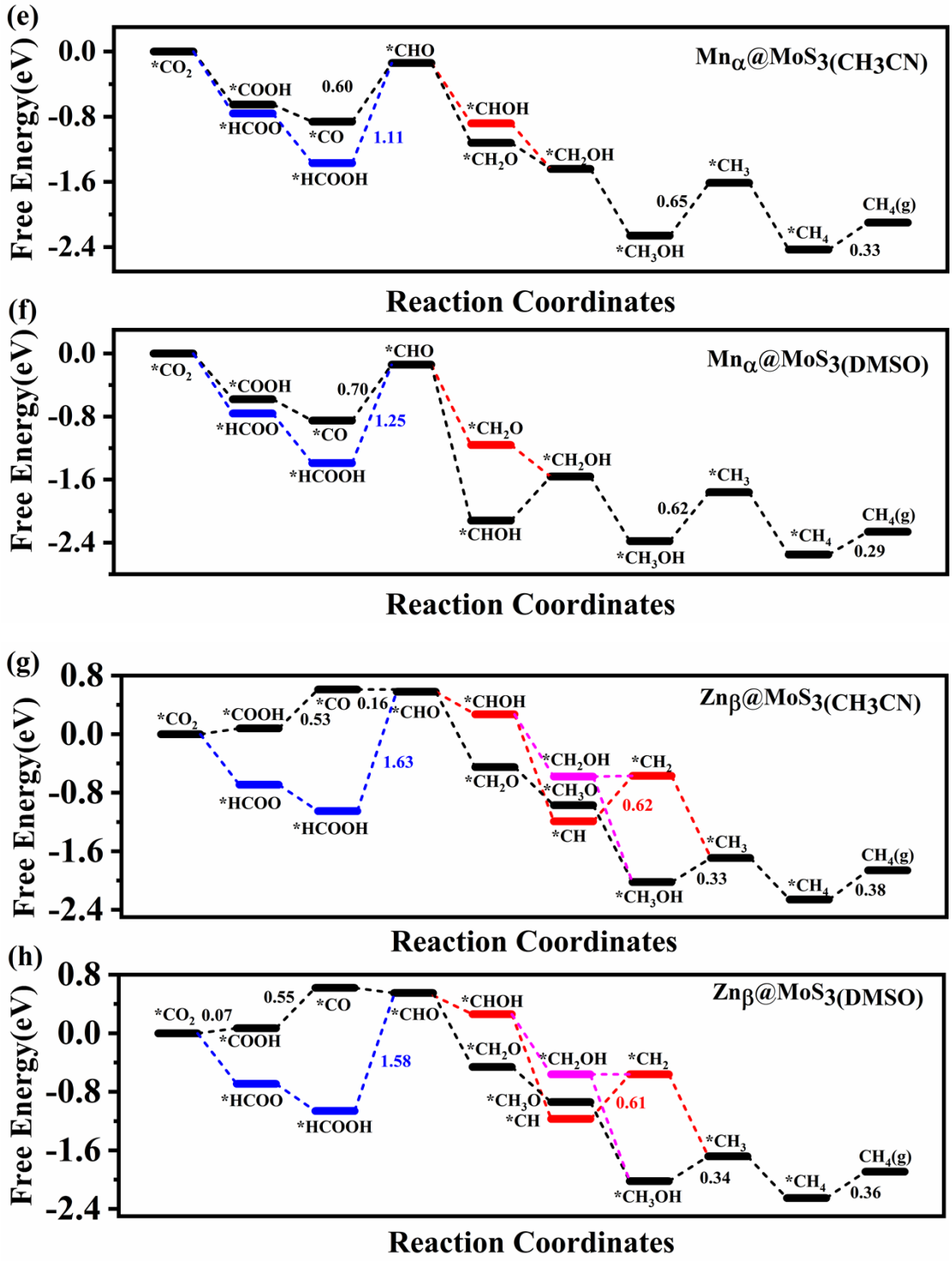

Fig. S7 Gibbs free energy changes for the protonation step of CO_2 reduction on various catalysts in CH_3CN and DMSO models: (a,b) $Co_\alpha@MoS_3$, (c,d) $Ni_\alpha@MoS_3$, (e,f) $Mn_\alpha@MoS_3$ and (g,h) $Zn_\beta@MoS_3$ catalysts in CH_3CN and DMSO models. The asterisk (*) indicates the intermediate species undergoing chemical adsorption.

To rigorously validate our computational framework and delineate the influence of dielectric screening, we performed a comprehensive analysis of the reaction

pathways using implicit solvation models with systematically varied dielectric constants (ε), specifically water (ε = 78.54), dimethyl sulfoxide (DMSO, ε = 46.826), and acetonitrile (MeCN, ε = 35.688). The key findings from this comparative study robustly affirm the physical insights presented in the main text.

The intrinsic product selectivity of each catalyst, producing either HCOOH (Co_α@MoS_3, Ni_α@MoS_3) or CH_4 (Mn_α@MoS_3, Zn_β@MoS_3), remains invariant across all solvent environments, demonstrating that the fundamental catalytic function is an inherent property of the doped active site. The identity of the rate-determining step (RDS) is largely conserved. For instance, the desorption process *HCOOH → HCOOH persists as the RDS for both Co_α@MoS_3 and Ni_α@MoS_3 regardless of ε, while the initial hydrogenation step (*CO_2 → *COOH) consistently presents the highest barrier for Zn_β@MoS_3. Notably, a subtle shift in the precise RDS for Mn_α@MoS_3 is observed when transitioning from the aqueous to the organic solvent models, yet this does not alter the overall mechanistic sequence or the final product. Although the absolute RDS barrier values exhibit a solvent-dependent modulation, with the aqueous model generally yielding the lowest barriers, attributable to its superior stabilization of charged transition states, the relative activity trend across the different metal dopants remains quantitatively consistent. Furthermore, this multi-model comparison clarifies how solvation fine-tunes certain microscopic pathway details without perturbing the overarching catalytic cycle.

In conclusion, while the dielectric constant of the implicit solvent influences the absolute energetics and refines certain mechanistic details, the core conclusions regarding product selectivity, the nature of the primary kinetic bottleneck, and the comparative catalyst performance hierarchy derived from the aqueous model (ε = 78.54) are exceptionally robust. This systematic validation underscores that the reported structure-activity relationships are intrinsic to the catalyst design and not an artifact of the chosen solvation framework.